Evolving air-sea interaction over the Nordic and Barents Seas and its impact on water mass transformation

Authors: G.W.K. Moore[1*], K. Våge[2], I.A. Renfrew[3] and R.S. Pickart[4]

Manuscript submitted to *Nature Climate Change*

June 12, 2020

[1]Department of Physics, University of Toronto, Canada

[2]Geophysical Institute, University of Bergen and Bjerknes Centre for Climate Research, Bergen, Norway

[3]School of Environmental Sciences, University of East Anglia, Norwich, UK

[4]Woods Hole Oceanographic Institution, Woods Hole, Massachusetts, USA

[*]Corresponding author: gwk.moore@utoronto.ca

The Nordic and Barents Seas play a critical role in the global climate system as a result of water mass transformation, triggered by intense air-sea heat fluxes, that is an integral component of the Atlantic Meridional Overturning Circulation (AMOC). These seas are undergoing rapid warming, associated with a significant retreat in ice cover, that is impacting regional ecosystems and the ocean convection that occurs within the Greenland and Iceland Seas. Here we present a novel analysis of the spatiotemporal variability of the air-sea heat fluxes along the region's boundary currents, where the most significant impacts on the overturning oceanic circulation are focused. We find recent trends towards higher air-sea heat fluxes – by up to 30% of the 40-year winter means – along these currents, implying enhanced water mass transformation. The enhanced transformation may be a transient situation, associated with sea ice retreat, or persist as a consequence of the reduced sea ice state. This needs to be considered to ascertain how the AMOC will respond to a warming climate.

The northward transport of warm and salty water within the North Atlantic Ocean, emanating from the Gulf Stream system, plays a fundamental role in the Earth's climate[1,2]. The wintertime densification of this Atlantic Water, via the transfer of heat and moisture to the atmosphere as it passes through the Nordic (Norwegian, Greenland and Iceland) and Barents Seas, is an important contributor to the deep southward return flow of the AMOC[1,3,4]. This water mass modification produces "Atlantic-origin overflow water" along the rim current system encircling the Nordic Seas [4]. In addition, colder and fresher "Arctic-origin overflow water" is formed within the interior basins of the western Nordic Seas[5-7]. Atlantic Water also enters the Arctic Ocean through Fram Strait and the Barents Sea[8,9] where it is further transformed[10], impacting the thermohaline structure of the Arctic Ocean, as well as the distribution of sea ice[11]. Ultimately this modified Atlantic Water reenters the Nordic Seas through Fram Strait where it contributes to

overflow waters crossing the Greenland-Scotland Ridge[4,5,12]. The regional air-sea interaction has an important impact on the atmosphere through a warming and moistening of the atmospheric boundary layer[13] and on marine ecosystems[14].

Within the Nordic and Barents Seas, there exist three major boundary currents where water mass modification occurs (Figure 1): the East Greenland Current (EGC) that flows southward along the East Greenland shelf break / upper-slope from Fram Strait to Denmark Strait[15]; the Norwegian Atlantic Current that flows northward through Fram Strait into the Nansen Basin as the Svalbard Branch (SB)[9,10]; and the Barents Sea Branch (BSB) that progresses from the Norwegian Sea through the Barents Sea towards Novaya Zemlya[8,16]. These latter two branches merge in the Arctic Ocean to form the circumpolar Atlantic Water Boundary Current. Water mass modification also occurs throughout the central Nordic Seas, most notably within the Norwegian Sea's Lofoten Basin[17] as well as within the Iceland and Greenland Seas[3,6,12]. Both the EGC and SB flow along the shelf break and this characteristic was used to define these current's domains, while for the BSB a representation of its spatial extent[18] was used. For all three currents, we assumed a width of 100km.

Most studies addressing the retreat of Arctic sea ice have focused on the loss of multi-year ice during September, when the extent is at its minimum[19]. However, here there has also been a significant decrease in sea-ice extent during winter. This can be seen by comparing the winter (November-April) mean sea-ice concentration[20] for the entire period 1979-2020 (Fig 2a) with that for the first and second halves of the period (Fig 2c&e). The retreat is substantial along the east coast of Greenland where it has resulted in the disappearance of the Odden Ice Tongue[21], as well as over the northern and eastern parts of the Barents Sea[22] and to the north of Svalbard[23]. The trends in winter mean sea-ice concentration (Figs. 2b,d,f) indicate a recent acceleration in ice loss

66 especially over the northern and eastern Barents Sea, the southwest Greenland Sea, and the western
67 Iceland Sea.

68 There is evidence that this retreat is leading to a reduction in air-sea interaction over the
69 central Iceland and Greenland Seas that may be lessening the production of dense overflow
70 waters[12,24]. At the same time, this is potentially exposing the EGC to the atmosphere leading to
71 enhanced air-sea interaction in that region[25]. Within the Barents Sea, the retreat of winter sea ice
72 has resulted in profound changes in the climate – an 'Atlantification' of the region[26].

73 Figure 2 clearly shows that the retreat of winter mean sea ice over the Nordic and Barents
74 Seas has occurred in the vicinity of the three boundary currents in question. This motivates an
75 examination of the spatiotemporal variability of air-sea heat fluxes along these currents. To
76 accomplish this, the 5th generation reanalysis from the European Centre for Medium-Range
77 Forecasts (ECMWF) known as ERA5 is used[27]. Both ERA5 and the well-established 4th generation
78 reanalysis known as ERA-Interim[28] are based on ECMWF's Integrated Forecast System (IFS). A
79 comparison with in-situ observations indicates that IFS-based datasets are able to represent the air-
80 sea fluxes in these subpolar seas with a good degree of fidelity[29-31]. The complex spatial
81 heterogeneity of the marginal ice zone leads to mesoscale variability in the air-sea heat fluxes[32]
82 that is not fully captured in reanalysis datasets[33]. To assess the impact of this uncertainty, a number
83 of sensitivity tests were performed that involved merging the native ERA5 air-sea heat fluxes with
84 those from the COARE bulk flux parameterization as a function of ice concentration. These tests
85 provided sufficient confidence in the ERA5 air-sea heat fluxes within the marginal ice zone for
86 this study. The ERA5 data have a spatial resolution of ~30 km and temporal resolution of 3 hours
87 for the period 1979-2020. The convention used is that fluxes out of the ocean are positive.

Figure 3 shows the spatiotemporal variability in the winter mean surface turbulent heat flux (the sum of the sensible and latent heat fluxes). The winter mean turbulent heat flux (Fig 3a) is small over ice covered regions as a result of the insulating properties of sea ice[34] and increases rapidly across the marginal ice zones with maxima in the northern Greenland Sea in the vicinity of Svalbard[12,24,35]. There are also minima in the Iceland and Greenland Seas that are the result of the competing influences of the two climatological low-pressure systems, the Icelandic and the Lofoten Lows, that are prevalent in the region during winter[35].

A change in the spatial distribution of the air-sea heat fluxes is clear in the trend of this field between 1979-1999 and 2000-2020 (Figs 3b&c). There is generally an increase in the turbulent heat flux in regions where there has been a loss of sea ice (c.f. Figs 2d&f). During the period 1979-1999 (Fig 3b), this is most pronounced over the western Greenland Sea, in the region of the Odden Ice Tongue, and over the central Barents Sea. From 2000-2020 (Fig 3c), there are more substantial trends over the northeastern Barents Sea, the northwestern Barents Sea / southern Nansen Basin, as well as the southwestern Greenland Sea and western Iceland Sea. In the interior of the Nordic Seas, including the location of the former Odden Ice Tongue, there is a near-uniform decrease in turbulent heat fluxes.

These geographical differences in the turbulent heat flux trend are the result of two distinct effects. In regions where there has been a loss of sea ice, the ocean has been exposed to the atmosphere allowing for an increased transfer of heat and moisture across the interface and hence a positive trend in winter[24]. Away from these regions, the trend towards lower air-sea heat fluxes is because the atmosphere is warming more rapidly than the ocean, leading to a smaller sea-air temperature difference (Supp. Fig 1). Idealized climate model experiments have shown that sea-

ice retreat is important for the Iceland Sea, while differential warming is dominant for the Greenland Sea[36].

Figure 3 also reveals that the areas of largest air-sea flux trend overlap with the boundary currents where water mass modification occurs. To quantify this, time series of the winter mean turbulent heat flux averaged over each of the boundary current segments (see Figure 1) are shown in Figure 4. Given the time-varying trends in Figure 3, linear or piecewise linear fits to the time series are overlaid. The choice of fit – and corresponding breakpoint – were determined from a low-frequency reconstruction of the time series generated by the Singular Spectral Analysis (SSA) technique[37]. The statistical significance of the trends was assessed using a Monte Carlo technique that uses 10,000 synthetic time series generated so as to retain the spectral characteristics of the underlying time series, thereby retaining any temporal autocorrelation that may reduce the degrees of freedom[24]. A 15-year moving window standard deviation is also shown for each time series as a measure of the inter-annual variability.

All three currents have a statistically significant increase in surface turbulence heat fluxes over time. In the EGC time series (Fig 4a) the trend is ~8 W m^{-2} $decade^{-1}$ after 2004 and is associated with a decrease in the magnitude of the inter-annual variability from ~20 Wm^{-2} to ~11 W m^{-2}. In the SB time series (Fig 4b) the trend is ~22 W m^{-2} $decade^{-1}$ after 2004 and is associated with an increase in the magnitude of the inter-annual variability from ~9 W m^{-2} to ~15 W m^{-2}. In the BSB time series (Fig 4c) the trend is ~8 W m^{-2} $decade^{-1}$ throughout the entire period with no apparent change in the magnitude of the inter-annual variability. The changes in inter-annual variability are driven by qualitative changes in wintertime sea ice in these regions. In the EGC region the inter-annual presence or absence of the Odden Ice tongue in the first two decades[21] dictates high variability in heat fluxes, compared to the latter decades when it is completely absent.

Similarly, a trend towards higher month-to-month variability in the Barents Sea ice cover[38] accounts for the higher variability in heat fluxes there.

The loss of sea ice and associated change in turbulent heat fluxes along these currents has not been uniform. This is demonstrated by constructing Hovmöller plots of the anomaly in the turbulent heat flux (Fig. 5). In the EGC (Fig 5a), there is a transition from a regime characterized by large inter-annual variability, with anomalies of either sign extending the length of the current, to one of mostly positive anomalies, especially along the southern extent of the current towards Denmark Strait (i.e. distances > 800 km; Fig.1). In the SB (Fig 5b) there is a change in behavior around 2007. Prior to this, the heat fluxes along the southern extent of the current (up to ~400 km) tended to be positive and out of phase with those along the northern extent. After the transition, the anomalies to the north are generally positive, extensive, and stronger, associated with negative anomalies to the south. Similar results also hold for the BSB starting around 2005, with a division at ~ 700 km (Fig 5c).

The magnitudes of these heat flux anomalies are substantial – as large as 30% of the winter mean values (Fig. 3a). Locally, the decadal changes are up to 20% for the EGC; up to 300% for the SB; and up to 200% for the BSB (Supp. Fig. 2). These changes are associated with the retreat of sea ice that is now exposing portions of these currents to the atmosphere (Supp Fig 3). Concomitant, there has been differential warming of the atmosphere and ocean, leading to a decrease in the sea-air temperature difference (Supp. Fig. 1), which would imply a decrease in surface sensible heat fluxes. However, for the boundary currents this is outweighed by the impact of the retreating sea ice.

It is likely that the increase in the magnitude of the turbulent heat flux along the three boundary currents is a transient response as the currents transition from one sea-ice regime to

another (Supp. Fig. 3). Once the wintertime sea ice has permanently retreated from a region, the differential warming of the atmosphere and ocean will lead to a decrease in the air-sea heat fluxes – as already evident along the southern sections of SB and BSB (Figs. 3, 5). We would anticipate these reduced fluxes will extend northward over time, and that the higher variability seen in the SB and BSB (Fig. 4) should continue, due to synoptic-scale atmospheric variability.

Previous work[24] has shown that the trend towards lower heat fluxes within the central basins is leading to shallower oceanic mixed-layers that are reducing the volume of the overturned waters. This in turn has the potential to reduce the ventilation of intermediate waters in the region, as well as to reduce the supply of dense overflow waters to the North Atlantic. In contrast, the reduction in ice and increased heat fluxes along the boundary currents has the potential to further ventilate and densify the Atlantic Water being transported by these currents. This has recently been observed along the southern EGC[25]. Our results place these observations in a longer-term context. Shifts in the region of enhanced air-sea interaction may also impact atmospheric phenomena such as polar lows[39] and cold-air outbreaks[40] – pushing the genesis of these northwards, consistent with Zahn and von Storch (2010).

The enhanced boundary current transformation implicated in this study has far-reaching consequences. The EGC supplies roughly half the overflow water to the North Atlantic Deep Western Boundary Current. Moreover, recent work has demonstrated that the largest contribution to the AMOC comes from the transformation that occurs in the Nordic Seas[41]. Further densification of this water will therefore restructure the AMOC by increasing its deep limb. This process needs to be considered in order to more accurately predict how the global overturning will respond to a warming climate. With regard to the SB and BSB, these two currents together supply warm and salty Atlantic Water to the Arctic Ocean. Increased densification within these currents will lead to

changes in the structure of the deep halocline of the Arctic Ocean, possibly altering the magnitude and depth range of the flux of this water into the interior. The enhanced heat loss as the water first enters the Nansen Basin could also impact the fate of the downstream ice cover, since less heat will be available for mixing into the surface waters. Going forward, more attention needs to be paid to the response of high latitude boundary currents as the wintertime ice recedes from the continental margins.

References

1 Rhines, P., Häkkinen, S. & Josey, S. A. in *Arctic–Subarctic Ocean Fluxes: Defining the Role of the Northern Seas in Climate* (eds Robert R. Dickson, Jens Meincke, & Peter Rhines) 87-109 (Springer Netherlands, 2008).

2 Kuhlbrodt, T. *et al*. On the driving processes of the Atlantic meridional overturning circulation. *Reviews of Geophysics* **45** (2007).

3 Marshall, J. & Schott, F. Open-ocean convection: Observations, theory, and models. *Reviews of Geophysics* **37**, 1-64, doi:10.1029/98rg02739 (1999).

4 Mauritzen, C. Production of dense overflow waters feeding the North Atlantic across the Greenland-Scotland Ridge .1. Evidence for a revised circulation scheme. *Deep-Sea Research Part I-Oceanographic Research Papers* **43**, 769-806, doi:10.1016/0967-0637(96)00037-4 (1996).

5 Våge, K. *et al*. Significant role of the North Icelandic Jet in the formation of Denmark Strait overflow water. *Nature Geoscience* **4**, 723 (2011).

6 Brakstad, A., Våge, K., Håvik, L. & Moore, G. Water Mass Transformation in the Greenland Sea during the Period 1986–2016. *Journal of Physical Oceanography* **49**, 121-140 (2019).

7 Swift, J. H. & Aagaard, K. Seasonal transitions and water mass formation in the Iceland and Greenland seas. *Deep Sea Research Part A. Oceanographic Research Papers* **28**, 1107-1129 (1981).

8 Smedsrud, L. H. *et al*. The role of the Barents Sea in the Arctic climate system. *Reviews of Geophysics* **51**, 415-449 (2013).

9 Våge, K. *et al*. The Atlantic Water boundary current in the Nansen Basin: Transport and mechanisms of lateral exchange. *Journal of Geophysical Research: Oceans* **121**, 6946-6960 (2016).

10 Pérez-Hernández, M. D. *et al*. Structure, Transport, and Seasonality of the Atlantic Water Boundary Current North of Svalbard: Results From a Yearlong Mooring Array. *Journal of Geophysical Research: Oceans* **124**, 1679-1698, doi:10.1029/2018jc014759 (2019).

11 Rudels, B. Arctic Ocean circulation and variability-advection and external forcing encounter constraints and local processes. *Ocean Science* (2012).

12 Våge, K., Moore, G. W. K., Jónsson, S. & Valdimarsson, H. Water mass transformation in the Iceland Sea. *Deep Sea Research Part I: Oceanographic Research Papers* **101**, 98-109 (2015).

13 Renfrew, I. A. *et al*. The Iceland Greenland Seas Project. *Bulletin of the American Meteorological Society* **100**, 1795-1817, doi:10.1175/BAMS-D-18-0217.1 (2019).
14 Loeng, H. & Drinkwater, K. An overview of the ecosystems of the Barents and Norwegian Seas and their response to climate variability. *Deep-Sea Research Part Ii-Topical Studies in Oceanography* **54**, 2478-2500, doi:10.1016/j.dsr2.2007.08.013 (2007).
15 Håvik, L. *et al*. Evolution of the East Greenland current from Fram Strait to Denmark strait: synoptic measurements from summer 2012. *Journal of Geophysical Research: Oceans* **122**, 1974-1994 (2017).
16 Sandø, A. B., Nilsen, J., Gao, Y. & Lohmann, K. Importance of heat transport and local air-sea heat fluxes for Barents Sea climate variability. *Journal of Geophysical Research: Oceans* **115** (2010).
17 Richards, C. G. & Straneo, F. Observations of Water Mass Transformation and Eddies in the Lofoten Basin of the Nordic Seas. *Journal of Physical Oceanography* **45**, 1735-1756, doi:10.1175/jpo-d-14-0238.1 (2015).
18 Lien, V. S., Schlichtholz, P., Skagseth, Ø. & Vikebø, F. B. Wind-driven Atlantic water flow as a direct mode for reduced Barents Sea ice cover. *Journal of Climate* **30**, 803-812 (2017).
19 Stroeve, J. C. *et al*. The Arctic's rapidly shrinking sea ice cover: a research synthesis. *Climatic Change* **110**, 1005-1027, doi:10.1007/s10584-011-0101-1 (2012).
20 Cavalieri, D. J., Parkinson, C. L., Gloersen, P., Comiso, J. C. & Zwally, H. J. Deriving long-term time series of sea ice cover from satellite passive-microwave multisensor data sets. *Journal of Geophysical Research: Oceans* **104**, 15803-15814, doi:10.1029/1999jc900081 (1999).
21 Comiso, J. C., Wadhams, P., Pedersen, L. T. & Gersten, R. A. Seasonal and interannual variability of the Odden ice tongue and a study of environmental effects. *Journal of Geophysical Research-Oceans* **106**, 9093-9116, doi:10.1029/2000jc000204 (2001).
22 Onarheim, I. H. & Årthun, M. Toward an ice-free Barents Sea. *Geophysical Research Letters* **44**, 8387-8395 (2017).
23 Onarheim, I. H., Smedsrud, L. H., Ingvaldsen, R. B. & Nilsen, F. Loss of sea ice during winter north of Svalbard. *Tellus A: Dynamic Meteorology and Oceanography* **66**, 23933, doi:10.3402/tellusa.v66.23933 (2014).
24 Moore, G. W. K., Våge, K., Pickart, R. S. & Renfrew, I. A. Decreasing intensity of open-ocean convection in the Greenland and Iceland seas. *Nature Climate Change* **5**, 877 (2015).
25 Våge, K., Papritz, L., Håvik, L., Spall, M. A. & Moore, G. W. K. Ocean convection linked to the recent ice edge retreat along east Greenland. *Nature communications* **9**, 1287 (2018).
26 Arthun, M., Eldevik, T., Smedsrud, L. H., Skagseth, O. & Ingvaldsen, R. B. Quantifying the Influence of Atlantic Heat on Barents Sea Ice Variability and Retreat. *Journal of Climate* **25**, 4736-4743, doi:10.1175/jcli-d-11-00466.1 (2012).
27 Hersbach, H. *et al*. The ERA5 Global Reanalysis. *Quarterly Journal of the Royal Meteorological Society* **n/a**, doi:10.1002/qj.3803.
28 Dee, D. P. *et al*. The ERA-Interim reanalysis: configuration and performance of the data assimilation system. *Quarterly Journal of the Royal Meteorological Society* **137**, 553-597, doi:10.1002/qj.828 (2011).

29 Renfrew, I. A., Moore, G. W. K., Guest, P. S. & Bumke, K. A comparison of surface layer and surface turbulent flux observations over the Labrador Sea with ECMWF analyses and NCEP reanalyses. *Journal of Physical Oceanography* **32**, 383-400 (2002).
30 Renfrew, I. A. *et al*. A comparison of aircraft-based surface-layer observations over Denmark Strait and the Irminger Sea with meteorological analyses and QuikSCAT winds. *Quarterly Journal of the Royal Meteorological Society* **135**, 2046-2066, doi:10.1002/qj.444 (2009).
31 Harden, B., Renfrew, I. & Petersen, G. Meteorological buoy observations from the central Iceland Sea. *Journal of Geophysical Research: Atmospheres* **120**, 3199-3208 (2015).
32 Fairall, C. W. & Markson, R. Mesoscale variations in surface stress, heat fluxes, and drag coefficient in the marginal ice zone during the 1983 Marginal Ice Zone Experiment. *Journal of Geophysical Research: Oceans* **92**, 6921-6932, doi:10.1029/JC092iC07p06921 (1987).
33 Inoue, J., Hori, M. E., Enomoto, T. & Kikuchi, T. Intercomparison of surface heat transfer near the Arctic marginal ice zone for multiple reanalyses: A case study of September 2009. *Sola* **7**, 57-60 (2011).
34 Moore, G. W. K., Schweiger, A., Zhang, J. & Steele, M. Collapse of the 2017 Winter Beaufort High: A Response to Thinning Sea Ice? *Geophysical Research Letters* **45**, 2860-2869, doi:10.1002/2017gl076446 (2018).
35 Moore, G. W. K., Renfrew, I. A. & Pickart, R. S. Spatial distribution of air-sea heat fluxes over the sub-polar North Atlantic Ocean. *Geophysical Research Letters* **39**, doi:10.1029/2012gl053097 (2012).
36 Pope, J. O., Bracegirdle, T. J., Renfrew, I. A. & Elvidge, A. D. The impact of wintertime sea-ice anomalies on high surface heat flux events in the Iceland and Greenland Seas. *Climate Dynamics*, doi:10.1007/s00382-019-05095-3 (2020).
37 Ghil, M. *et al*. Advanced spectral methods for climatic time series. *Reviews of Geophysics* **40**, doi:10.1029/2000rg000092 (2002).
38 Cavalieri, D. J. & Parkinson, C. L. Arctic sea ice variability and trends, 1979-2010. *The Cryosphere* **6**, 881 (2012).
39 Landgren, O. A., Batrak, Y., Haugen, J. E., Støylen, E. & Iversen, T. Polar low variability and future projections for the Nordic and Barents Seas. *Quarterly Journal of the Royal Meteorological Society* **145**, 3116-3128, doi:10.1002/qj.3608 (2019).
40 Papritz, L. Arctic Lower-Tropospheric Warm and Cold Extremes: Horizontal and Vertical Transport, Diabatic Processes, and Linkage to Synoptic Circulation Features. *Journal of Climate* **33**, 993-1016, doi:10.1175/JCLI-D-19-0638.1 (2019).
41 Chafik, L. & Rossby, T. Volume, Heat, and Freshwater Divergences in the Subpolar North Atlantic Suggest the Nordic Seas as Key to the State of the Meridional Overturning Circulation. *Geophysical Research Letters* **46**, 4799-4808 (2019).

Acknowledgements

The authors would like to thank the European Centre for Medium-Range Weather Forecasts for access to the ERA5. G.W.K.M. was supported by the Natural Sciences and Engineering Research

Council of Canada. K.V. has received funding from the Trond Mohn Foundation (BFS2016REK01) I.A.R. has received funding from the Natural Environmental Research Council for the AFIS project (NE/N009754/1). R.S.P. was supported by the US National Science Foundation. This study arose from discussions during the Iceland Greenland Seas Project.

Author contributions

G.W.K.M., K.V., I.A.R and R.S.P. jointly conceived the study. G.W.K.M. analysed the atmospheric reanalyses and sea-ice data sets. K.V. and R.S.P. developed the current domains. All authors jointly interpreted the results and wrote the manuscript.

Additional information

Supplementary information is available in the online version of the paper. Reprints andpermissions information is available online at www.nature.com/reprints. Correspondence and requests for materials should be addressed to G.W.K.M.

Competing financial interests

The authors declare no competing financial interests.

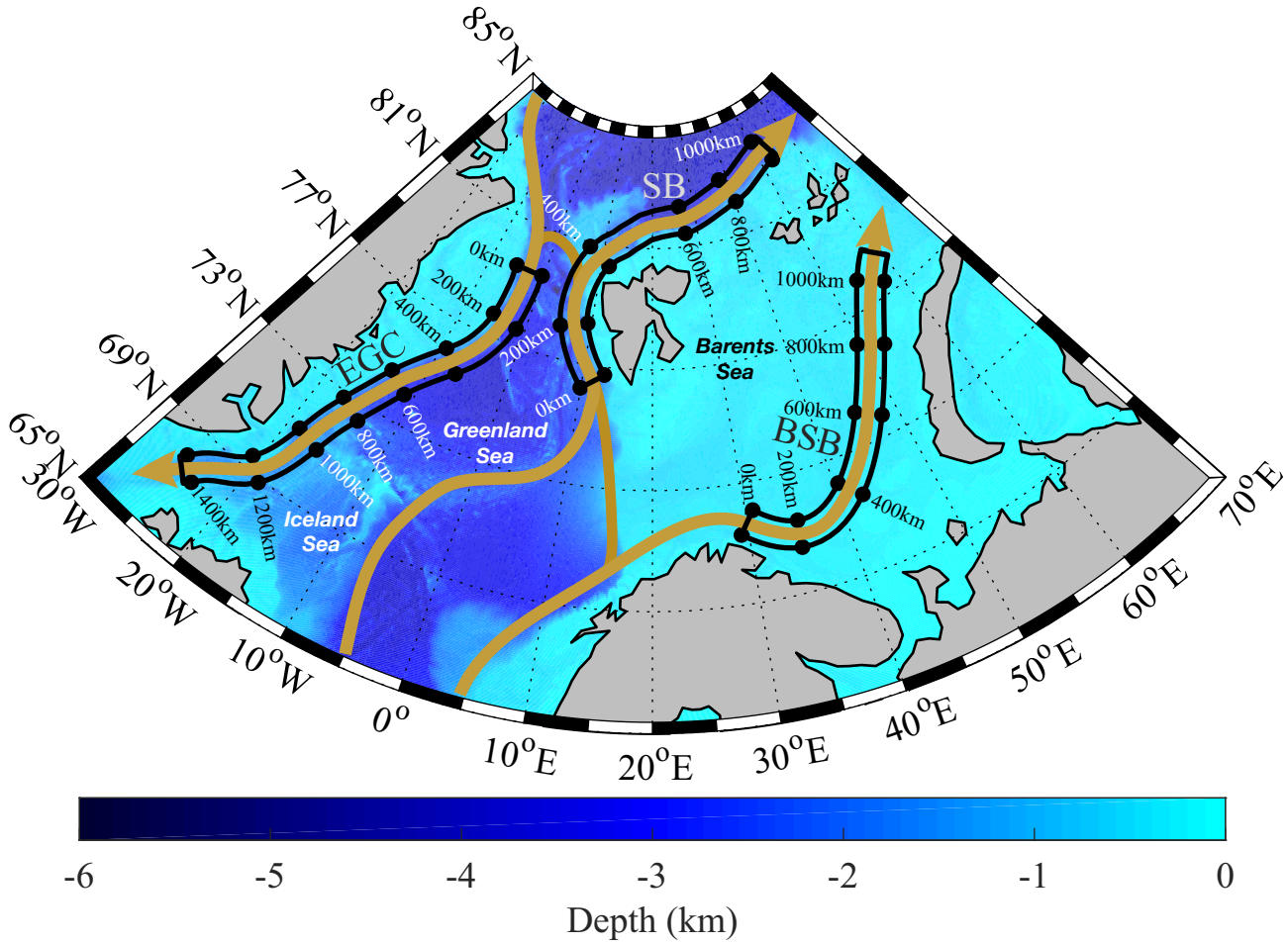

Figure 1) The bathymetry (km) of the Nordic and Barents Seas. The domains associated with the East Greenland Current (EGC) , the Svalbard Branch (SB) and the Barents Sea Branch (BSB) of the Atlantic Water Boundary Current are shown in black with distances along the direction of the current flow indicated.

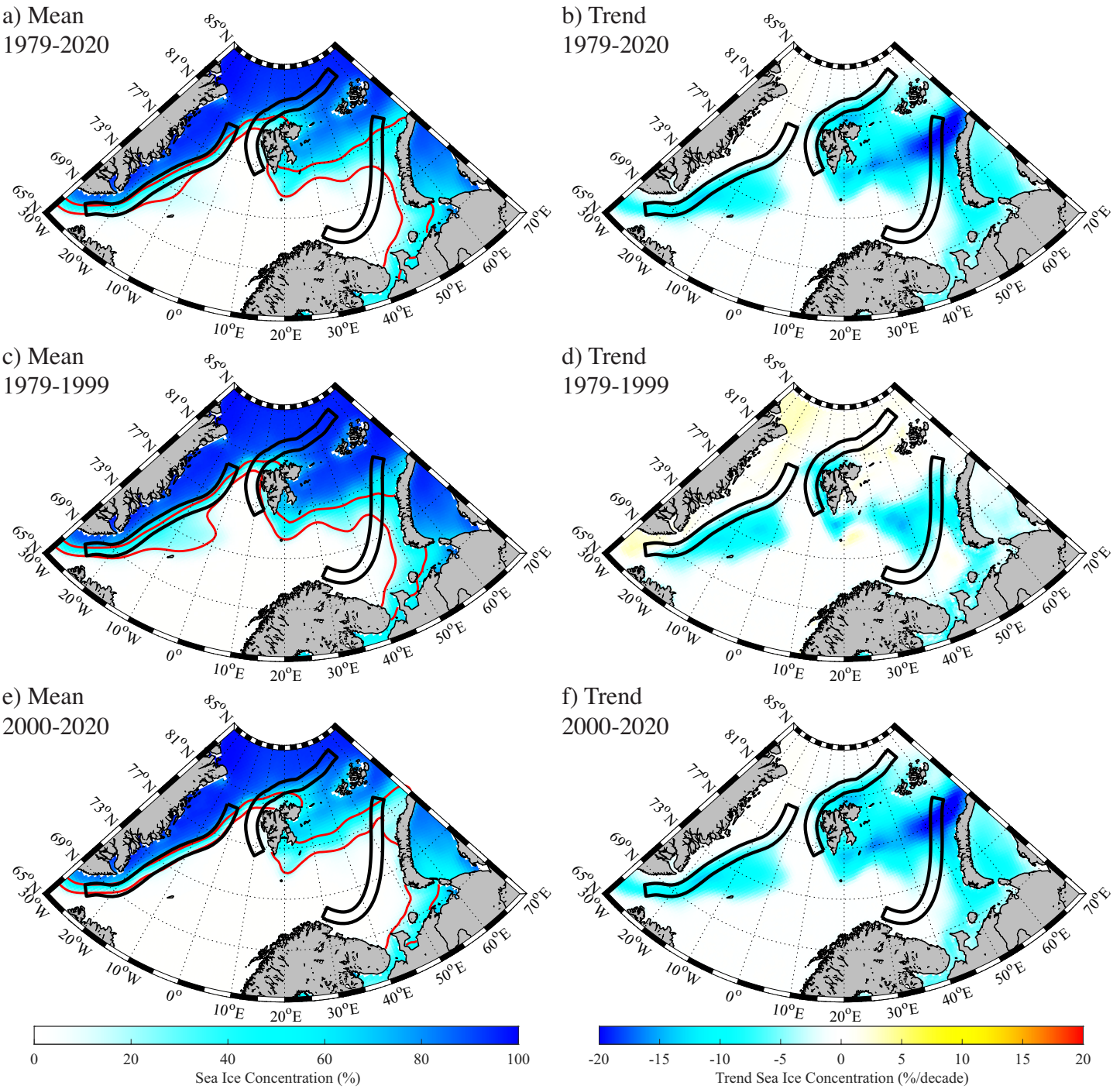

Figure 2) Spatiotemporal variability in sea ice concentration over the Nordic and Barents Seas in winter (November to April). The mean (%; left column) and trends (% decade^{-1}; right column) are shown for: a),b) 1979-2020; c),d) 1979-1999; e),f) 2000-2020. The domains associated with the EGC, and the SB and BSB of the Atlantic Water Boundary Current are shown in black. The 15% and 50% sea ice concentration contours are shown in red in the left column.

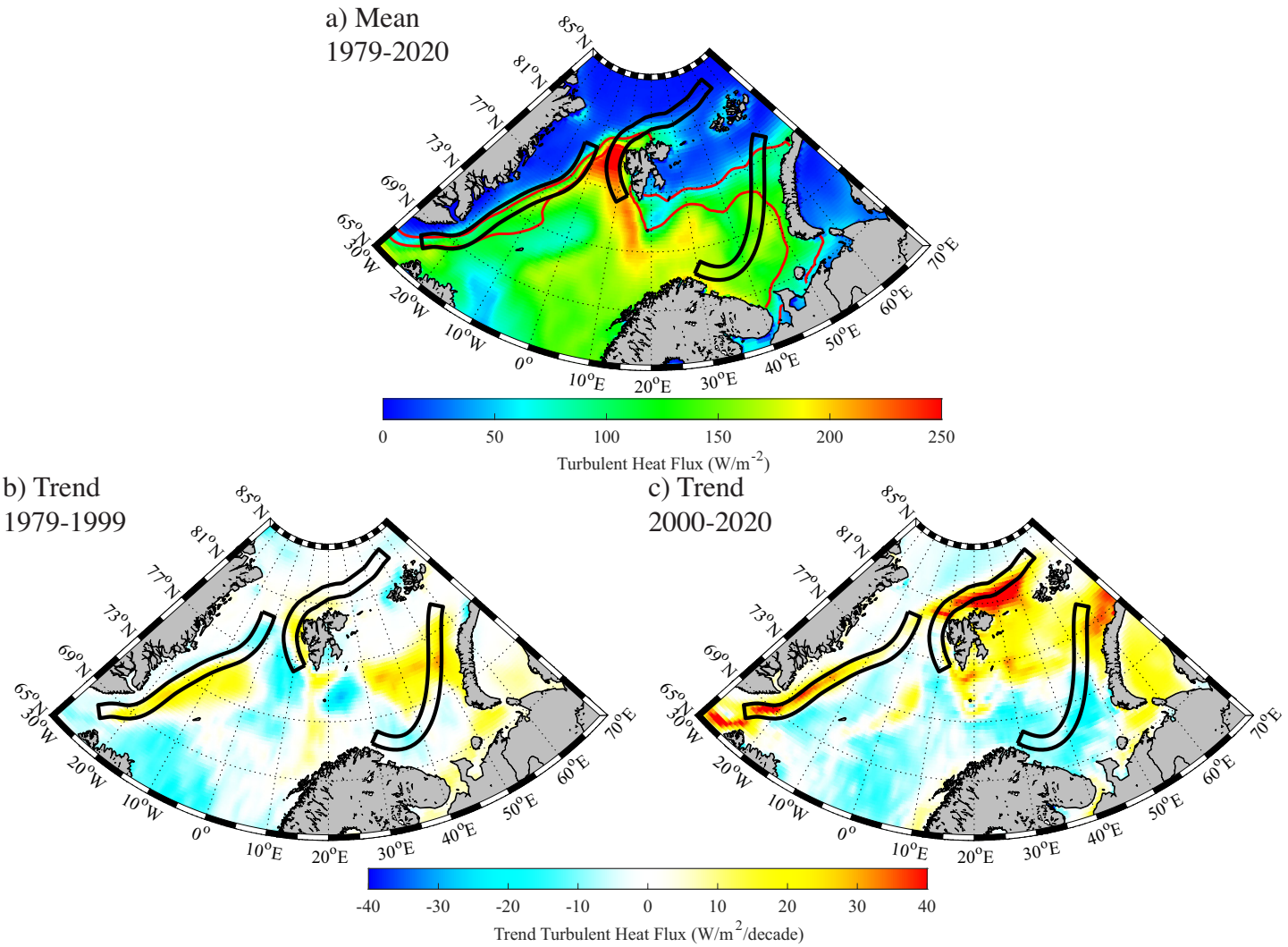

Figure 3) Spatiotemporal variabilty in turbulent heat flux over the Nordic and Barents Seas in winter. Panels show a) the mean (W m^{-2}) for 1979-2020; and the trends (W m^{-2} $decade^{-1}$) for b) 1979-1999; and c) 2000-2020. The domains associated with the EGC, and the SB and BSB of the Atlantic Water Boundary Current are shown in black. The 15% and 50% sea ice concentration contours are shown in red in a).

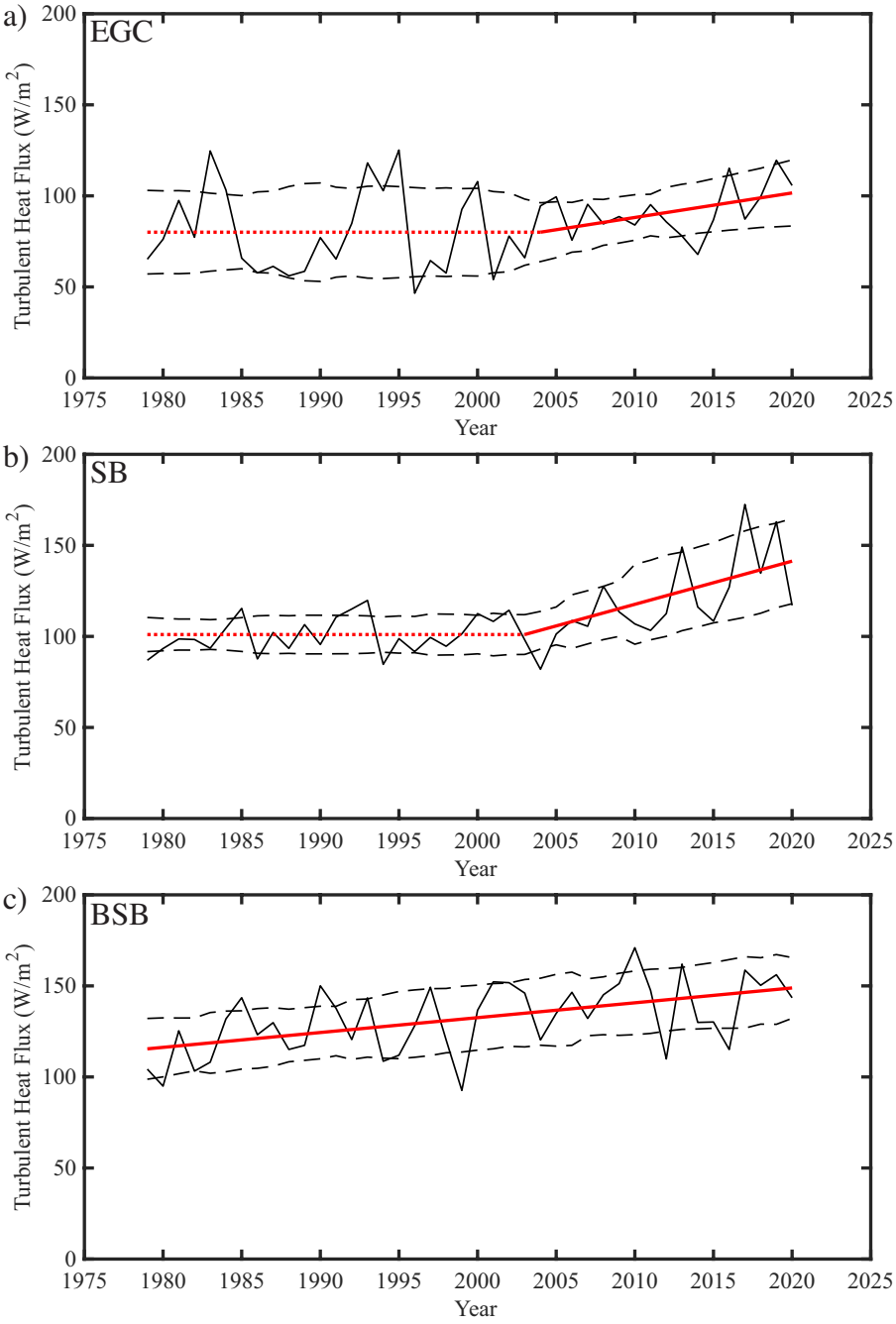

Figure 4) Time series of winter mean turbulent heat flux (W m^{-2}) over a) the East Greenland Current; b) the Svalbard Branch; and c) the Barents Sea Branch of the Atlantic Water Boundary Current. Linear or piecewise linear least-square fits to the time series are shown in red, with trends that are statistically significant indicated by the solid lines. Interannual variability, using a 15-year moving window standard deviation, is shown via the dashed black curves.

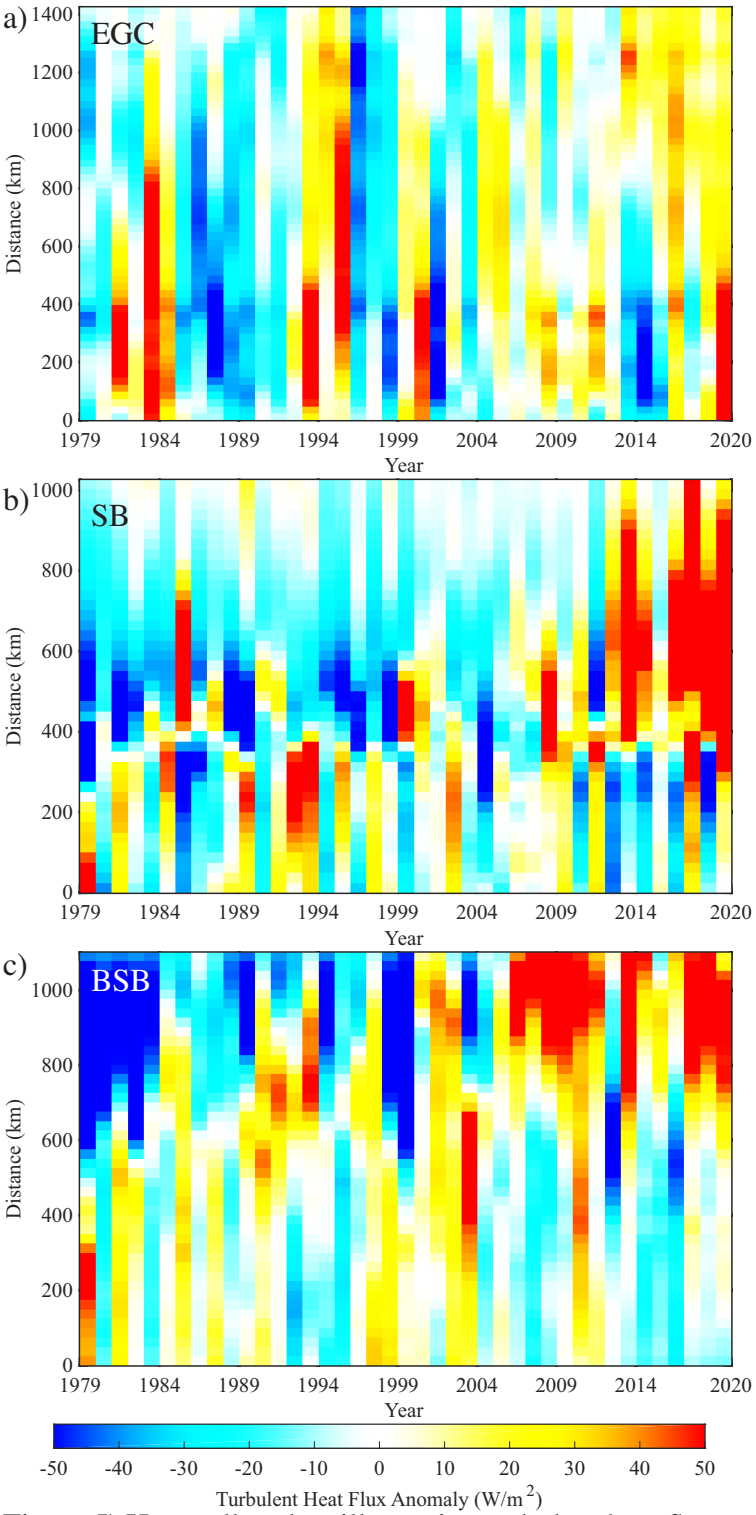

Figure 5) Hovmöller plots illustrating turbulent heat flux anomaly (W m-2) with respect to year and distance along the current. Panels are for a) EGC; b) SB and c) BSB. The anomaly is an annual anomaly with respect to the mean from 1979-2020.

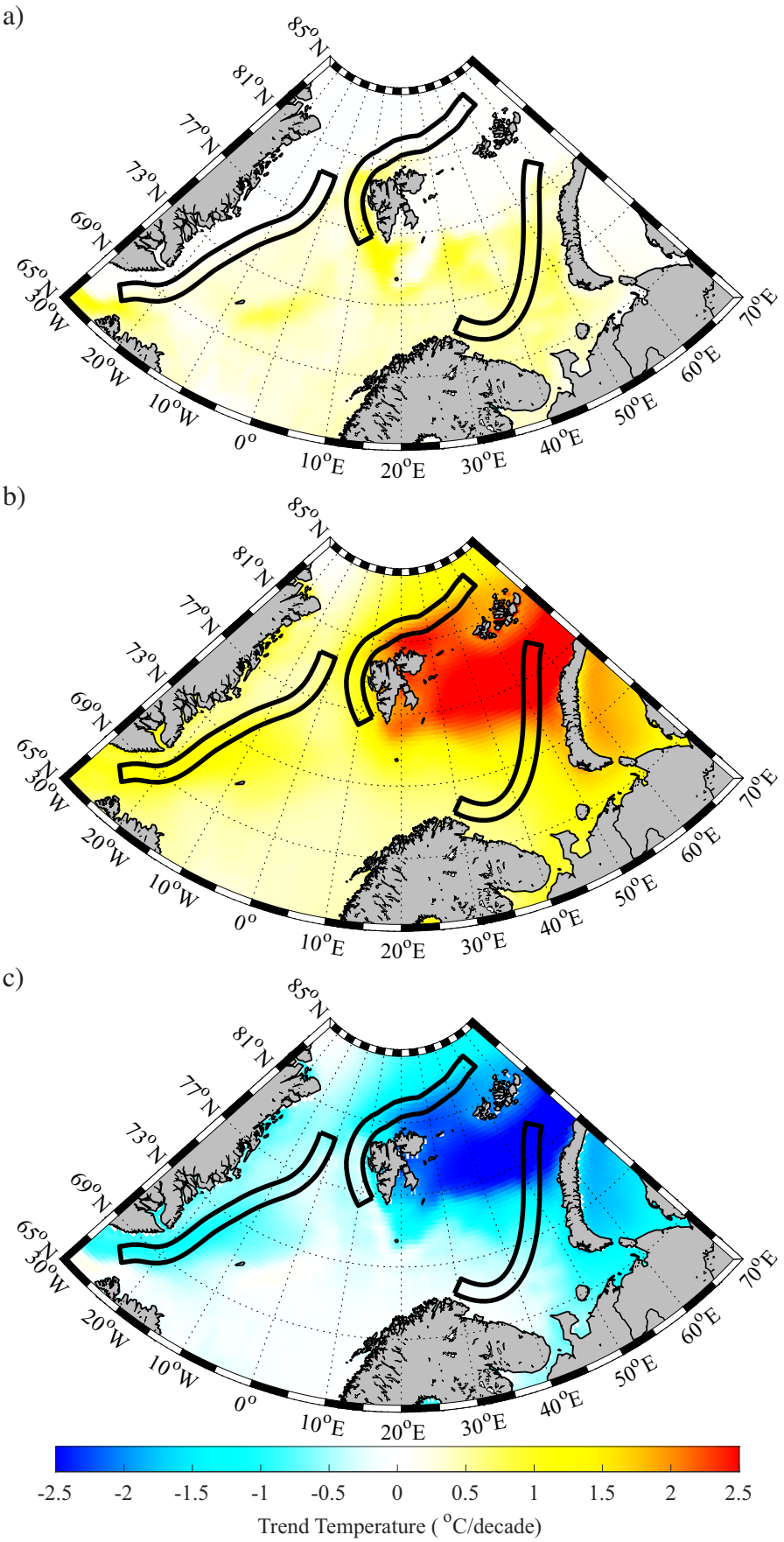

Supplementary Figure 1 | Trends in winter mean meteorological variables for the period 1979-2020: a) 2-m air temperature; b) sea surface temperature; and c) sea-air temperature difference. All trends are in K decade^{-1} using ERA5 data.

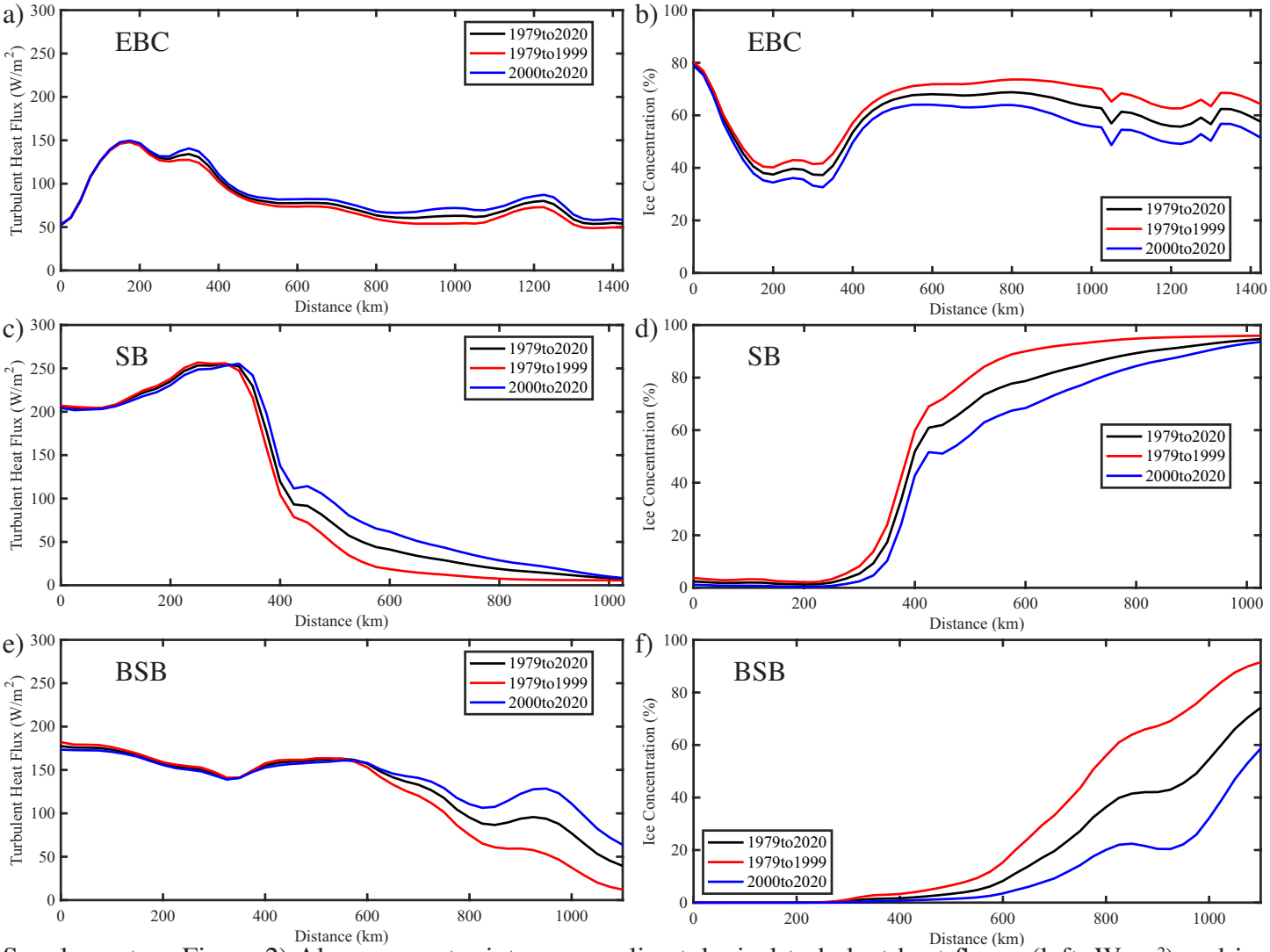

Supplementary Figure 2) Along-current winter mean climatological turbulent heat fluxes (left; W m^{-2}) and ice concentration (right; %). The panels are for the a),b) EGC; c),d) SB; e),f) BSB. The black curves are for the period 1979-2020, while the red and blue curves are for 1979-1999 and 2000-2020 respectively.

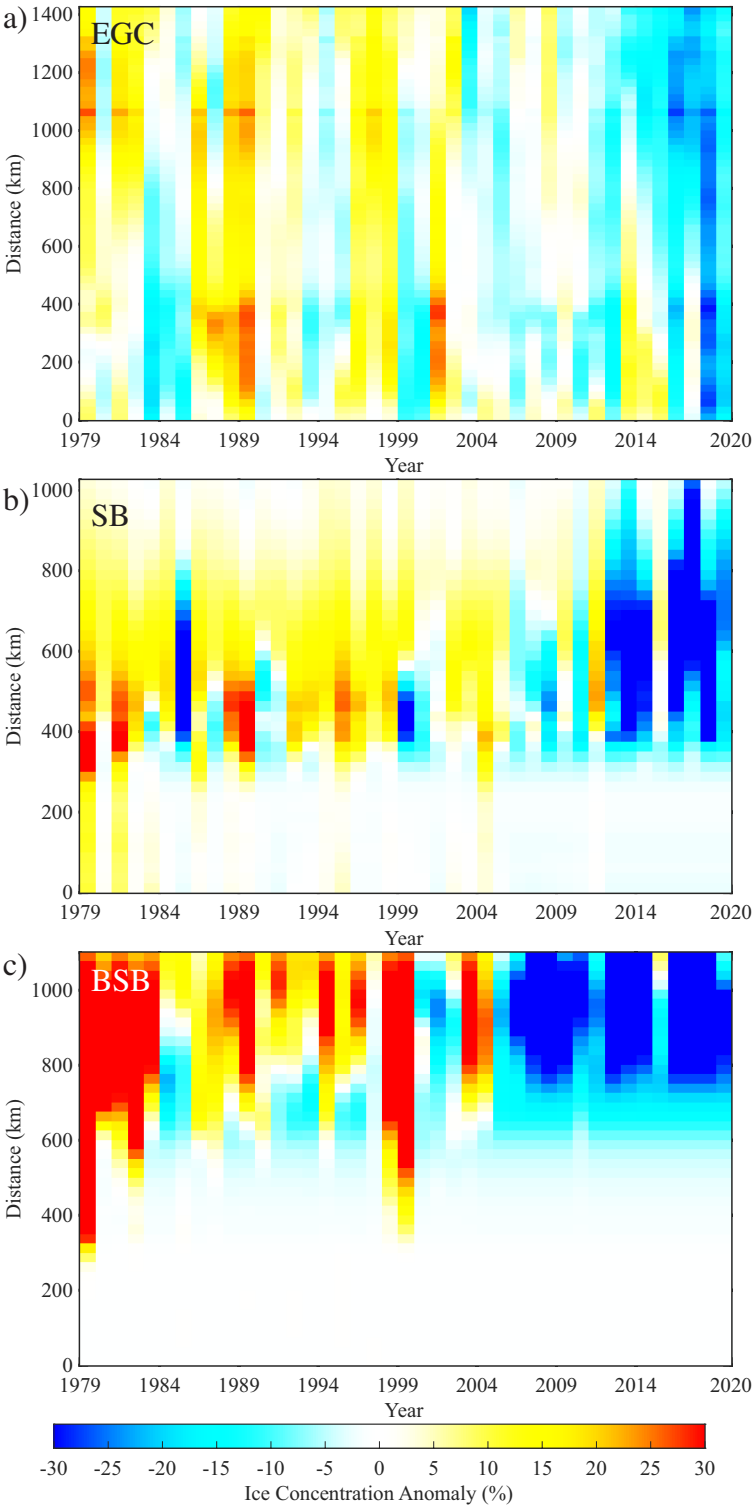

Supplementary Figure 3) Hovmöller plots illustrating ice concentration anomaly (%) with respect to year and distance along the current. Panels are for a) EGC; b) SB and c) BSB. The anomaly is an annual anomaly with respect to the mean from 1979-2020.